Check for updates

Chemistry
Europe

European Chemical
Societies Publishing

VIP *Very Important Paper*

Special
Collection

The Charged Linker Modulates the Conformations and Molecular Interactions of Hsp90

Abraham López,[a, b] Annika R. Elimelech,[b] Karolin Klimm,[b] and Michael Sattler*[a, b]

Dedicated to Prof. Horst Kessler on the occasion of his 80th birthday.

The molecular chaperone Hsp90 supports the functional activity of specific substrate proteins (clients). For client processing, the Hsp90 dimer undergoes a series of ATP-driven conformational rearrangements. Flexible linkers connecting the three domains of Hsp90 are crucial to enable dynamic arrangements. The long charged linker connecting the N-terminal (NTD) and middle (MD) domains exhibits additional functions *in vitro* and *in vivo*. The structural basis for these functions remains unclear. Here, we characterize the conformation and dynamics of the linker and NTD–MD domain interactions by NMR spectroscopy. Our results reveal two regions in the linker that are dynamic and exhibit secondary structure conformation. We show that these regions mediate transient interactions with strand β8 of the NTD. As a consequence, this strand detaches and exposes a hydrophobic surface patch, which enables binding to the p53 client. We propose that the charged linker plays an important regulatory role by coupling the Hsp90 NTD–MD arrangement with the accessibility of a client binding site on the NTD.

Introduction

The molecular chaperone Hsp90 has a crucial role in protein homeostasis. Distinct from most other chaperones, Hsp90 interacts with a specific set of substrates referred to as clients, helping them to achieve their active states.[1] Hsp90 is dimer where each protomer comprises three domains, the N-terminal domain (NTD, residues 1–210 in yeast), the middle domain (MD, 273–525), and the primary dimerization C-terminal domain (CTD, 534–610). In order to achieve its function, Hsp90 requires ATP binding to the NTD and subsequent hydrolysis with the assistance of a catalytic loop in the MD. ATPase activity is coupled to large conformational rearrangements of the chaperone, from an open conformation to a hydrolysis-competent closed state, through several intermediate steps.[2] Populations of open and closed states are distinct depending on the species,[3] but the timing between steps is a common and important determinant for the chaperone function.[4] Co-chaperones provide an additional degree of regulation of the Hsp90 conformational cycle by modulating specific Hsp90 conformations and their lifetimes.

Critical for the essential conformational cycle of Hsp90 is the presence of flexible linkers between constitutive domains, especially concerning the NTD–MD linker. The two domains are connected by a large, negatively charged linker (residues 211–272 in *Saccharomyces cerevisiae*, Figure 1A). Its length and sequence varies significantly between species, ranging from approximately ten residues for *Escherichia coli*, up to almost 100 in some eukaryotes. The presence of longer linkers in eukaryotes suggests that, besides providing interdomain flexibility, it has additional specific functions for the conformational response of Hsp90 upon substrate and co-chaperone binding.[5] In addition, the presence of several post-translational modifications in this region suggests further regulatory functions[6] (https://www.phosphosite.org).

Although previous studies have highlighted the functional relevance of the charged linker,[5b,7] the significance and important features for Hsp90 function remain unclear, especially due to the difficulties in its structural analysis. The intrinsic flexibility of the linker required its removal for crystallization,[2b] and precluded its detection in cryo-EM 3D reconstructions.[8] Some studies have addressed roles of the NTD–MD linker from a functional perspective. Deletion of residues 211–259 was found to support yeast viability similar to the wild-type protein, but the removal of residues 211–263 led to temperature sensitivity, while of residues 211–266 was inviable.[7b] The effects of replacing the linker regions of other organisms into yeast Hsp90 on cell viability were studied. Heat sensitivity and *in vitro* effects of clients and co-chaperones revealed that the linker sequence enables a more complex regulation of Hsp90 activity. In addition, substitution of the linker residues by uncharged Gly-Ser (GS) motifs negatively affected ATPase and stability of the NTD.[5b] Taken together, these studies indicate a critical function of the linker, but the molecular features required at amino acid level are unclear.

Crosslinking and fluorescence experiments with different linker deletions and substitutions showed that residues 259–

[a] Dr. A. López, Prof. Dr. M. Sattler
Institute of Structural Biology, Helmholtz Zentrum München
Ingolstädter Landstrasse 1, 85764 Neuherberg (Germany)
E-mail: sattler@helmholtz-muenchen.de

[b] Dr. A. López, A. R. Elimelech, K. Klimm, Prof. Dr. M. Sattler
Bavarian NMR Center and Center for Integrated Protein Science Munich
Department of Chemistry, Technical University of Munich
Lichtenbergstrasse 4, 85747 Garching (Germany)

Special
Collection *This article is part of a Special Collection on the occasion of Horst Kessler's 80th birthday. To view the complete collection, visit our homepage*

ChemBioChem

Full Papers
doi.org/10.1002/cbic.202000699

**Chemistry
Europe**
European Chemical
Societies Publishing

263 are important for providing sufficient rotational freedom of the NTD with respect to the MD. This interdomain flexibility is necessary for Hsp90 function,[9] ATPase activity and stimulation by the co-chaperone Aha1, but only required for the activity of certain clients. Single-molecule studies of Hsp90 unfolding by optical tweezers and FRET suggest the presence of transient NTD-linker interactions.[9b] These interactions were only possible in the presence of the wild-type linker sequence, while substitution by GS motifs resulted in increased dimer closure. It has been shown that linker modulates substrate peptide binding affinity to the NTD.[10] Deletion of the linker can reverse detrimental effects caused by mutations on the C-terminal strand of the domain *in vitro*.[11]

These observations suggest a regulatory role of the NTD-linker interactions. However, details about the structural properties, conformational dynamics and interactions of the linker at high resolution are still lacking. As is emerging for many multidomain proteins,[12] intrinsically disordered regions and linkers flanking globular domains play important roles for Hsp90 function. The conformational features of the linker are thus important for understanding interdomain arrangements and communication in the Hsp90 dimer, as well as interactions with substrates and co-chaperones. Here, we employ NMR spectroscopy to characterize the conformation and dynamics of the linker and investigate interactions with neighboring domains. Our results indicate the presence of partially structured regions in the linker. Unexpectedly, these linker regions mediate transient interactions with the NTD that lead to the exposure of interaction sites with Hsp90 binding partners, indicating important regulatory roles of the linker.

Results

Comparison of NTD- and MD-linker extensions

To investigate potential interactions between the linker and the NTD or MD of yeast Hsp90, we expressed constructs of the two domains with increasing linker lengths and analyzed their ^{1}H,^{15}N NMR correlation spectra. For this purpose, the linker was divided into three distinct regions (N-, mid- and C-linker) based on charge and hydrophobicity, sequence conservation and secondary structure propensity (Figure 1B–D). N-linker comprises residues 211–220 and the hydrophobic ^{217}VPIP^{220} motif. Mid-linker harbors a low-complexity region in which in Glu-Asp/Lys residues are abundant (38% Glu/Lys and 24% Asp within residues 221–241). This segment consists of four (D/E)(D/E)(D/E)KK tandem repeats with notable periodicity (20% deviation from perfect EEEKK motifs).[7b,13] The C-linker consists of an initial Lys-rich region (amino acids 253–261) followed by an alternation of negatively charged and hydrophobic residues (262–269). The constructs for the NTD and the MD comprised residues 1–217 and 273–529, respectively. Based on the structure of the full-length Hsp90 dimer (PDB ID: 2CG9[2b]) a short stretch of disordered residues is included in the NTD in order to ensure its structural integrity (residues 211–217). Domain extensions with the linker regions defined above resulted in NTD constructs

NTD_226, NTD_252 and NTD_274 (Figure 2A, top). Applying similar boundaries to N-terminal linker extensions of the MD yielded 252_MD, 226_MD and 210_MD constructs (Figure 2C, top). An additional construct studied comprises the NTD and MD domains connected by the native linker (NTD_MD, residues 1–529).

The ^{1}H,^{15}N correlation spectra of C-terminal linker extensions of the NTD show dispersed residues of the folded domain with minimal spectral changes compared to the minimal NTD, indicating that the overall structure is maintained (Figure 2A).
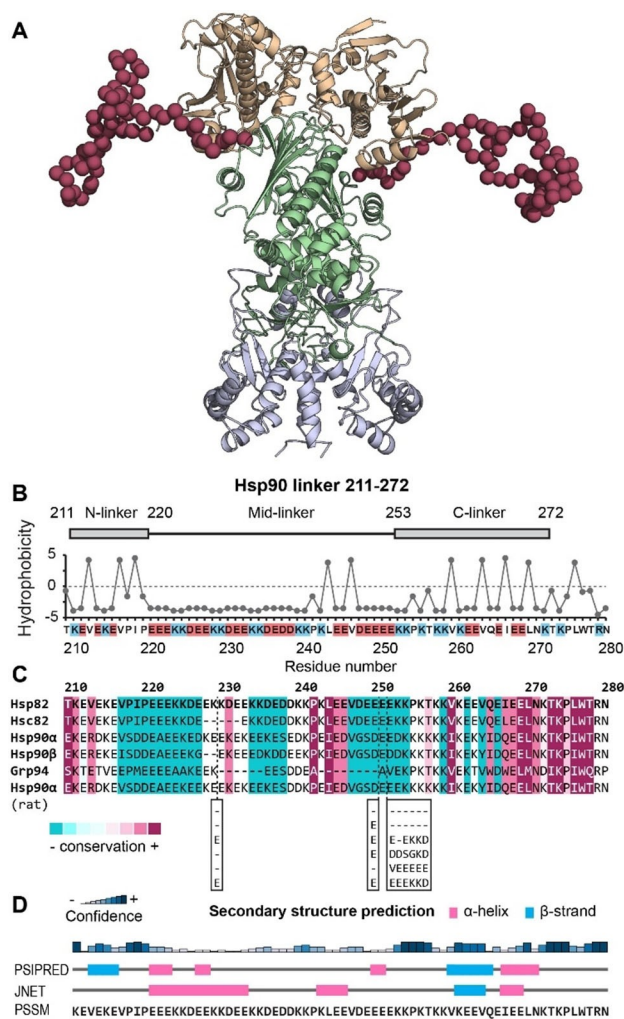

Figure 1. Hsp90 architecture and properties of the NTD–MD linker. A) X-ray structure of yeast Hsp90 (PDB ID: 2CG9[2b]) with the NTD–MD linker modeled in a random conformation by using Swiss-Model[14] with the crystallographic structure as input (dark red spheres). Constitutive domains are colored as follows: NTD in beige, MD in green, and CTD in lilac. B) Hydrophobicity (Kyte-Doolittle scale[15]) and charge distribution of yeast Hsp90 residues between 210 and 280. Blue and red indicate positively and negatively charged side-chain groups, respectively. The different segments of the linker (residues 211–272) are shown at the top, namely N-, mid- and C-linker. C) Hsp90 linker sequence alignment of different isoforms and organisms as well as conservation analysis using Consurf server:[16] yeast (isoforms Hsc82 and Hsp82), human (α, β and the endoplasmic reticulum Grp94), and rat Hsp90α. D) Secondary structure prediction by using PSIPRED[17] and JNETPSSM (Jpred[18]) servers. Pink and blue rectangles indicate helix and extended conformation prediction, respectively; the bar plot shows the confidence of PSIPRED prediction.

ChemBioChem

Full Papers
doi.org/10.1002/cbic.202000699

Chemistry
Europe
European Chemical
Societies Publishing

The central region of these spectra contains intense signals. These correspond to the linker residues with a narrow distribution of amide ^{1}H chemical shifts, pointing out the high degree of disorder of the linker. However, a careful examination of the disordered region reveals some particular features. In C-terminal extensions up to NTD_252, linker resonances show narrow linewidths and mostly appear as additional signals upon increasing linker length, without significant chemical shift changes between constructs (Figure 2B, top). Contrarily, the linker spectrum of NTD_274 shows severe line broadening, resulting in less observable peaks compared to NTD_252 (Figure 2B, bottom).
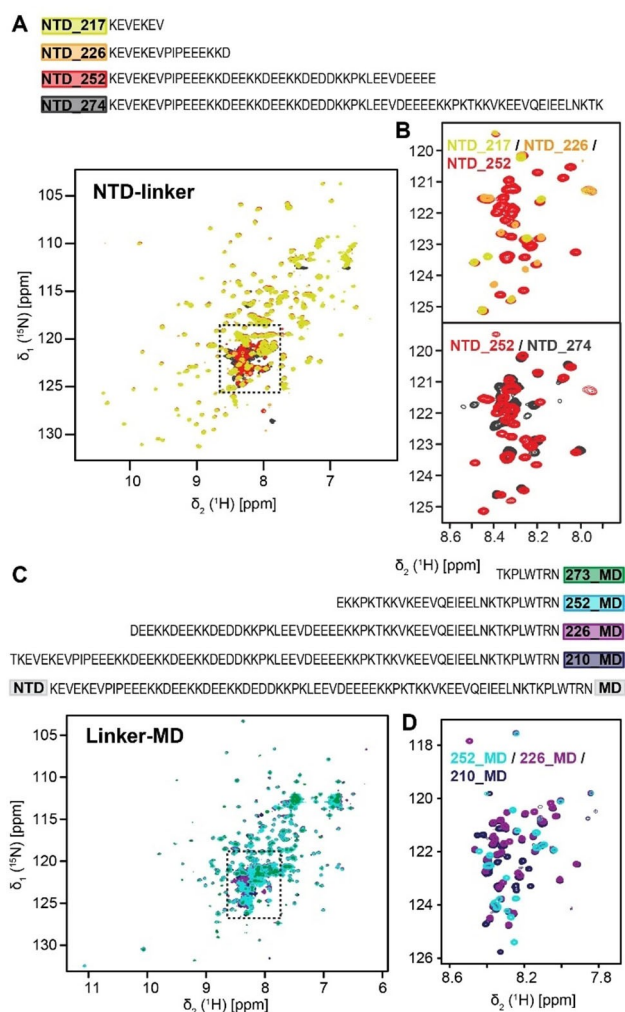
In N-terminal extensions of the MD, the presence of linker of increasing lengths does not cause significant variations on the disperse resonances corresponding to the folded domain (Figure 2C). As in the case of the NTD constructs, this indicates that the general fold of the MD is maintained independently of the linker. A closer look at the disordered region reveals that, in contrast to the NTD-linker constructs, all resonances are narrow and exhibit minimal chemical shift differences in all constructs (Figure 2D). Thus, differential line broadening seen in ^{1}H,^{15}N correlation spectra of different NTD- and MD-linker extensions suggest that residues 252–274 of the linker participate in transient interactions on the micro- to millisecond timescale involving the NTD, whereas no significant interactions occur between the linker and the MD.

N- and C-terminal linker regions contain residual secondary structure and mediate interactions with the NTD

Considering that the C-terminal linker exhibits transient interactions in the presence of the NTD, we next investigated which residues are involved, and if the presence of residual secondary structure could mediate such interactions. We expressed and purified a fragment comprising linker residues 210–283. Residues 273–283, which do not form part of the linker, were included to support the purification of the construct based on the UV absorbance of Trp277 at 280 nm. Control HSQC experiments with NTD_283 reveal a similar pattern of line broadening observed for NTD_274, demonstrating that the presence of this additional C-terminal extension does not perturb the linker interactions (data not shown). The ^{1}H,^{15}N HSQC spectrum of the isolated linker (Figure 3A) shows limited ^{1}H chemical shift dispersion and narrow linewidths of the amide signals consistent with its low structural content.

To map the interactions and assess the potential secondary structure propensity of the linker, we assigned the backbone chemical shifts using standard triple resonance experiments. Based on this, ^{13}C secondary chemical shifts were calculated for ^{13}Cα, ^{13}Cβ and ^{13}C' spins (Figure 3B). In addition, {^{1}H}^{15}N heteronuclear NOE values were measured to assess conformational flexibility on sub-nanosecond timescales. These data reveal two regions that exhibit residual secondary structure in the N-linker (residues 210–222) and C-linker (248–272) regions. In addition, residues 273–283 also display residual secondary structure. In contrast, the mid-linker (residues 223–247), which is comprised mostly by Glu-Asp/Lys repeats, shows little deviations from random coil chemical shifts and exhibits negative heteronuclear NOE values, indicating high flexibility. Negative ^{13}C secondary chemical shifts of the N-linker indicate propensity for an extended conformation, disrupted by the presence of Pro218 and Pro220. In contrast, the C-linker shows alternating stretches of helical motifs (^{250}EEEK^{253} and ^{267}IEELN^{271}) and random coil (residues 254–267). Interestingly, the second helical motif ^{268}EELNK^{272} corresponds to residues 280–284 forming a short helix in the cryo-EM structure of human Hsp90.[8] Heteronuclear NOE values close to zero in the two

Figure 2. Comparison of ^{1}H,^{15}N HSQC spectra of NTD- and MD-linker extension constructs. Spectra of A) NTD-linker and C) MD-linker constructs show a narrow ^{1}H chemical shift distribution of linker peaks (dashed boxes), indicating lack of stable secondary structure. Disperse peaks corresponding to the structured domains show minimal variations, thus indicating that the overall fold is not significantly perturbed by linker extension. B) A detailed view of the linker region discloses that resonances in NTD constructs up to NTD_252 are minimally perturbed (top). However, in construct NTD_274 (lower panel), significant line broadening and perturbations occurs, leading to less observable peaks compared to NTD_252. D) In contrast, linker resonances in all MD constructs show minimal perturbations and no line broadening.

ChemBioChem

Full Papers
doi.org/10.1002/cbic.202000699

Chemistry
Europe
European Chemical
Societies Publishing

helical regions are consistent with transient secondary structure formation in C-linker.

To characterize the interactions of the linker with the folded domains we transferred the assignments of the isolated linker to the NTD_274 and 210_MD constructs harboring the full linker (Figure 3C, D). We first assumed minimal chemical shift deviation for initial assignment and confirmed chemical shift assignments using backbone correlation experiments. With this approach, all linker resonances of 210_MD could be assigned up to position Leu 276, a point where line broadening and overlap with signals of the folded domain avoid further analysis. Comparison of spectra and analysis of chemical shift perturbations (CSPs) between the isolated linker and the 210_MD construct reveal minimal perturbations, except near the C-

terminal part due to the proximity of the folded domain (Figure 3C, E). In contrast, N- and C-linker signals are not observable in the NTD_274 construct. This indicates that amide signals in these two segments experience severe line broadening presumably due to dynamic interactions with the NTD. In contrast, all signals of the mid-linker region are readily observed and do not show any significant chemical shift differences comparing the NTD_274 and the isolated linker (Figure 3D, E), demonstrating that the mid-linker does not interact with the NTD.
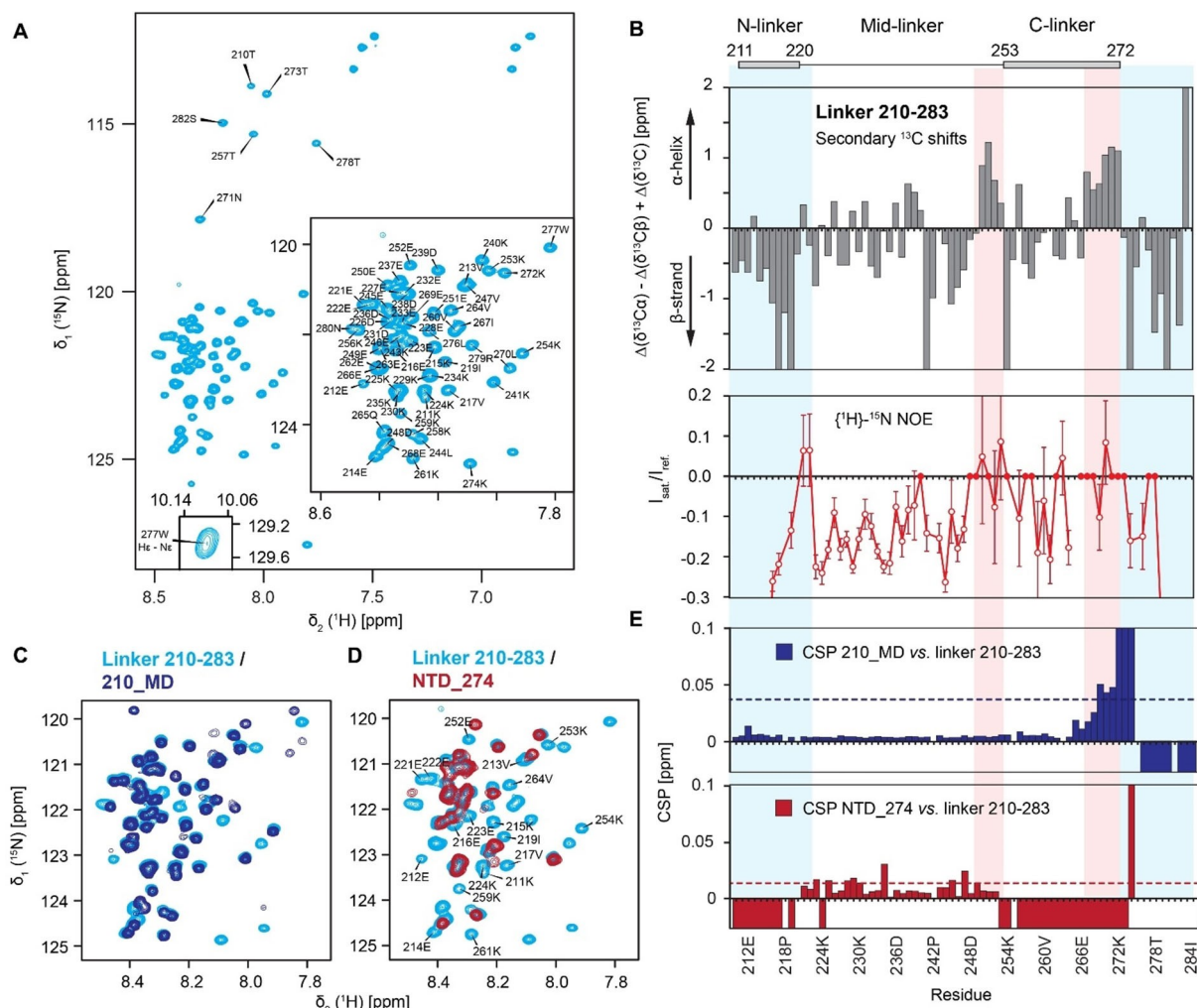

Figure 3. Backbone amide resonance assignment of Hsp90 NTD–MD linker, residual secondary structure and interactions with folded domains. A) $^1H,^{15}N$ HSQC spectrum of linker construct 210–283 showing assignments. The experiment was recorded at 600 MHz at a concentration of 150 μM. B) ^{13}C chemical-shift deviations of Cα, Cβ and C′ atoms with respect to random-coil values of the isolated linker (top). Positive and negative deviations in the ^{13}C chemical shifts reveal helical and extended conformation propensity, respectively (highlighted in red and blue). The corresponding {^1H}^{15}N heteronuclear NOE values are shown at the bottom. Non-negative heteronuclear NOE values indicate transient secondary structure; crosspeaks that were not observed in the saturated experiment were assigned to zero (filled circles). N-, mid- and C-linker boundaries are marked on the top. C), D) Spectral comparison of isolated linker (light blue) with 210_MD (C, dark blue) and NTD_274 (D, maroon). The high similarity of MD_210 reveals no significant interactions with the folded domain; in contrast, the severe line broadening in N- and C-linker peaks of NTD_274 indicates interactions on the micro- to millisecond timescale involving the folded domain. E) CSP plot of linker residues of 210_MD (dark blue) and of NTD_274 (maroon) with respect to isolated linker construct. Negative bars indicate unassigned residues due to line broadening; median $+1\sigma$ are marked as dotted lines.

ChemBioChem

Full Papers
doi.org/10.1002/cbic.202000699

Chemistry Europe
European Chemical
Societies Publishing

The C-terminal linker region interacts transiently with NTD causing β8 strand detachment

Next, we investigated which regions in the NTD mediate contacts with the linker. We transferred the available assignments of NTD and MD domains[19] and analyzed chemical shift and intensity differences between the isolated globular NTD and MD domains alone and in the presence of the linker extensions. Consistent with the lack of significant perturbations for 210_MD versus isolated linker, comparing 210_MD with 273_MD shows no detectable changes on the MD, thus indicating the absence of even transient interactions (data not shown). Comparison of NTD_217 and NTD_274, however, reveals significant local perturbations and line broadening as a result of linker interactions (Figure 4A, C). When mapped onto the crystal structure of the isolated NTD (PDB ID: 1AM1;[20] Figure 4B), strong CSPs and line-broadening cluster on strands

β2-β3 and the connecting turn, as well as on helix α8, in close spatial proximity. Severe line broadening of signals in the strand β8 (^{205}IQLV^{208}) at the C-terminal end of the NTD indicates that these residues experience significant dynamics on micro- to millisecond timescales.

In order to shed light into the structural basis of such perturbations, we recorded 3D CCH NOESY experiments of methyl labeled NTD_210 and NTD_MD proteins and analyzed the NOE pattern of residues in the affected regions. According to the crystal structure, intense NOEs between methyl groups in strands β2-β8 and helix α8-strand β8 are consistent with the formation of the strand β8 in NTD_210 (Figure 4D). In contrast, in the NTD_MD construct the absence of significant NOEs with residues in the β8 strand points to a substantial conformational difference. We hypothesize that C-linker interacts transiently with the β8 strand, and thereby weakens contacts of β8 with the β2 strand and helix α8. To provide further support for this
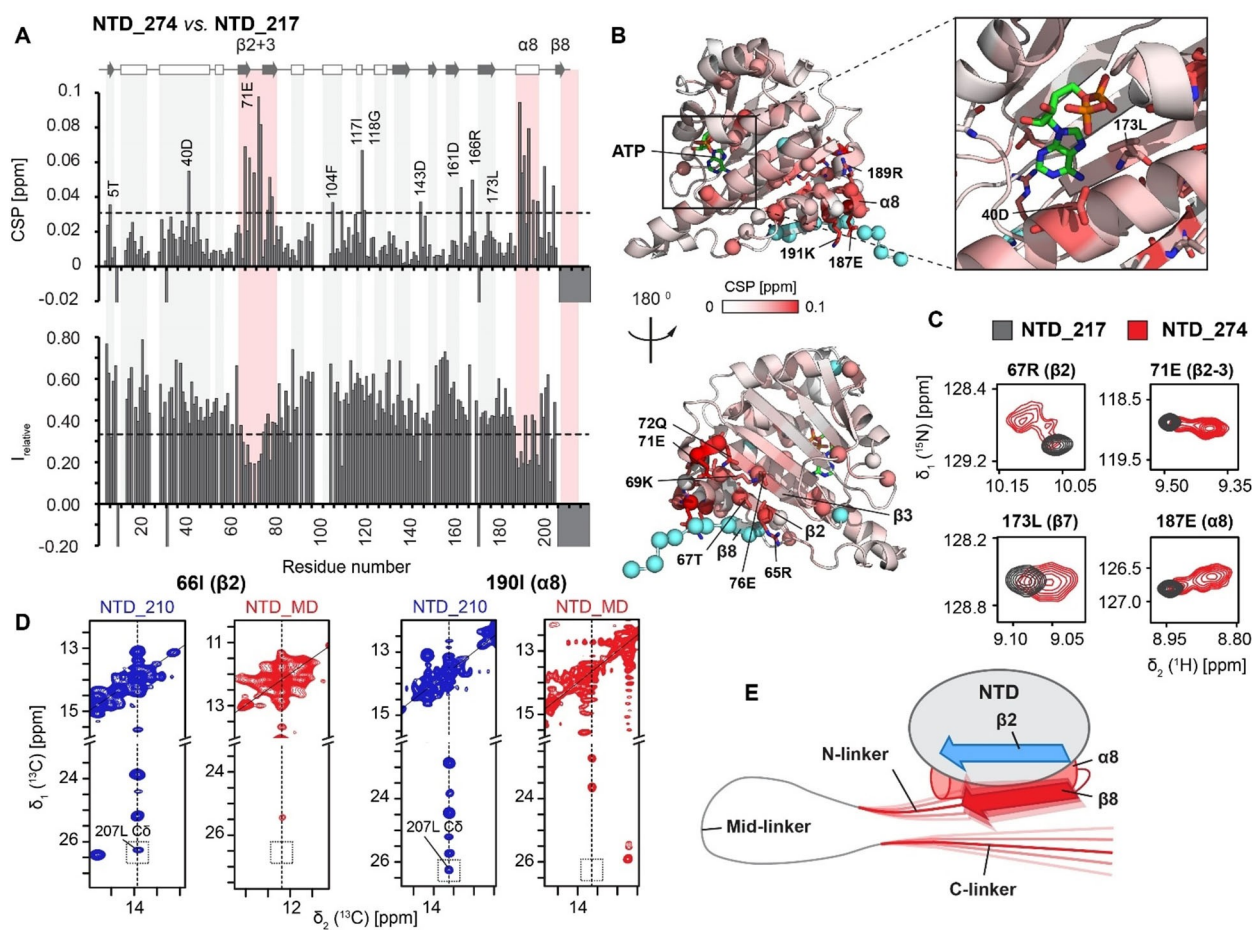

Figure 4. The C-linker binds transiently to the NTD and causes partial detachment of β8. A) CSP and intensity ratios of NTD_274 vs. NTD_217. Changes in β2, β3 and α8 (highlighted in red) indicate increased dynamics due to C-linker presence. Severe line broadening of β8 (negative bars) indicates the high dynamics of this element. Additional perturbations outside these regions are indicated on the plot. Median values + or −1σ are shown as dotted lines for CSP or relative intensities, respectively. B) Mapping of CSP and intensity ratios on the crystal structure of NTD bound to ATP (PDB ID: 1AM1[20]). Most perturbed residues are shown as spheres, and residues undergoing line broadening are colored in cyan. Side chains of residues affected by linker interactions are labeled and represented as sticks. The inset shows perturbations extending to neighboring elements α2 and β7 forming the ATP pocket. C) Detailed views of resonances of the ^{1}H,^{15}N HSQC spectra of NTD_217 and NTD_274 perturbed by linker contacts. D) ^{13}C,^{13}C strips of 3D CCH NOESY experiments showing inter-methyl NOEs of 66I (β2) and 190I (α8) with 207 L of β8 (labeled). The methyl NOEs observed in NTD_210 (dark blue) indicate stable sheet formation, whereas the absence of any detectable signals in NTD_MD (red) reveals lower stability and transient disruption of β8 (dashed boxes). E) Schematic representation of dynamic C-linker contacts with β8 and N-linker (red), leading to increased dynamics and partial disruption of β8 from β2 and α8.

ChemBioChem

Full Papers
doi.org/10.1002/cbic.202000699

**Chemistry
Europe**
European Chemical
Societies Publishing

hypothesis, we compared the CSPs and intensity ratios between NTD_217 and the NTD extension construct that lacks the C-linker region, that is, NTD_252. As seen in Figure S1 in the Supporting information, the absence of the C-linker (residues 253–273) no longer causes chemical shift changes or line broadening for amide signals in β2, α8 and β8 of the NTD. This confirms that the dynamic interaction of the C-linker segment is responsible for the detachment of β8. Further analysis of the chemical shift perturbations comparing NTD_217 versus NTD_274 highlights large spectral changes for the amide of Glu71, which is located in the turn between the β2 and β3 strands. As this residue is distant from β8, the observed chemical shift differences suggest that Glu17 might be important for interactions with the linker, probably through long-range electrostatic contacts. To support this hypothesis, we replaced Glu by Gln to remove the negative charge of the side chain and compared chemical shifts for NTD_217 E71Q with respect to the wild-type (Figure S2A, B). As expected, the removal of the charge does not induce significant changes in the folded domain except for neighboring residues, but nevertheless causes strong chemical shift changes for residues [209]VTKEV[215] flanking β8. Taken together, these results suggest that Glu71 interacts with the first residues of the N-linker region and thereby may stabilize the interaction of the β8 strand with the β2 strand in the NTD.

Destabilization of the β8 strand exposes a hydrophobic client binding site

The structural and dynamic effects of linker interactions with the NTD have potential consequences on the function and binding properties of the domain. The Hsp90 NTD is involved in client and co-chaperone interactions, for example, with the disordered substrate Tau,[21] the globular DNA-binding domain (DBD) of p53,[19c,22] and the ligand binding domain of the glucocorticoid receptor.[23] The NTD is also crucial for the binding and activity of the co-chaperones p23[2b,24] and Aha1,[25] among others. In fact, biochemical studies have shown that hydrophobic residues in the β8 strand contribute to interactions with clients and the co-chaperones p23 and Aha1.[11] The presence of an extension of the NTD with the subsequent linker enhances binding of substrate peptides, suggesting a regulatory role.[10] However, the underlying structural mechanisms of these observations are unclear.

Previous NMR studies using methyl labeling have identified that Ile218 and Ile214 in the human Hsp90α NTD are involved in binding to the p53-DBD.[22] Interestingly, these residues are located in strand β8 and the preceding loop of the NTD, respectively. We hypothesize that the exposure of hydrophobic residues in the β8 strand due to transient C-linker interactions enables contacts with clients to this site. In fact, the high content of hydrophobic residues in the region of amino acids 200–210 (average hydrophilicity value of 1.7 on the Kyte-Doolittle scale[15]) suggests a potential role of this stretch in substrate interactions. To validate this, we investigated the binding of the NTD extension construct NTD_274 to p53-DBD.

We prepared a 1:1 complex between NTD_274 and p53-DBD in the presence of ATP and monitored spectral changes induced by client binding in $^1H,^{15}N$ HSQC spectra. Binding of the client results in overall minor chemical shift changes and line broadening for some amides (Figure 5A). Consistent with previous studies,[19c,22] the absence of large spectral changes indicates that the substrate does not induce structural rearrangements in the NTD. However, the presence of distinct chemical shift changes and/or line broadening for several signals indicates transient and dynamic interactions associated with client binding (Figure 5A, D). Mapping of CSP and intensity ratios onto the crystal structure of NTD-ATP (PDB ID: 1AM1,[20] Figure 5B, C) reveals that the perturbations cluster to distinct regions in the NTD.

As previously described by Kessler and co-workers, p53 binding induces changes in the secondary dimerization helix α1 and the region formed by the N-terminal end of helix α2 and the ATP lid.[19c] Interestingly, additional CSPs are seen for strand β2 and the adjacent strands β3 and β7, and are accompanied by line broadening for some residues in α8 and β8. The absence of any significant spectral changes for signals in the linker indicates that the observed effects are due to direct substrate contacts and not a result of indirect effects or competitive binding of the substrate to the linker.

To unambiguously validate a role of NTD-linker interactions in exposing the β8 strand we formed the client complex with the minimal NTD_217 construct which lacks most of the linker. The lack of significant spectral changes in the NTD (Figure 5E, F) supports the role of a linker-induced destabilization of β8 for client binding. To rule out that the linker could affect the nucleotide binding affinity of the NTD and thereby interfere with client binding, we performed isothermal titration calorimetry (ITC) experiments comparing NTD_217 and NTD_274 (Figure S3). The ITC data show very similar affinities, enthalpy and entropic contributions upon ADP binding to the two constructs. This proves that transient linker interactions do not have a significant effect on nucleotide binding. Altogether, our results show that partial exposure of hydrophobic residues of strand β8 and its surroundings induced by transient linker contacts promotes the interaction with the p53 client.

Discussion

Here, we have performed a detailed NMR analysis of the conformational features and flexibility of the Hsp90 NTD–MD linker based on secondary ^{13}C chemical shifts and NMR relaxation data. Based on the NMR data and an analysis of the amino acid composition we defined three distinct regions in the linker: N-, mid- and C-linker. The N-linker, harboring a hydrophobic VPIP motif, shows β-sheet propensity. The high content of Glu-Asp/Lys residues of mid-linker, containing four imperfect EEEKK repeats, results in pronounced flexibility of the polypeptide in this region, judged by the absence of deviations in secondary ^{13}C chemical shifts and low heteronuclear NOE values. The C-linker shows high abundance of Lys and several hydrophobic residues and comprises two short stretches with

helical propensity. Notably, the amino acid features in the N- and C-linker regions are evolutionary conserved, whereas more sequence variations are found for the mid-linker region.

Comparative analysis of NMR data for NTD constructs with increasing linker lengths reveals dynamic interactions of N- and C-linker regions with the NTD, but no such interactions of the mid-linker. Transient contacts between linker and NTD have been proposed in previous studies,[9b] but the structural basis for such interactions remained unclear. Here, we show that the strand β8 of the NTD undergoes a highly dynamic interaction with the C-linker region, causing its destabilization and partial detachment from strand β2 and helix α8 in the NTD. This is consistent with a previous study showing that linker deletion reversed the effects of a destabilization of strand β8 by a I205A mutation in the NTD. As a consequence, ATPase activity, chaperone function and viability of the full length protein was restored.[11] NMR data indicate extensive interactions of the linker with the NTD involving multiple transient contacts. These are not only limited to β8, but extend to the N-linker and the complete C-linker, causing severe line broadening in these regions. In line with this, single-molecule experiments indicated that residues 264–272 are not sufficient for NTD-linker interactions.[9b] Furthermore, in some crystal structures of the full-length Hsp90 dimer, an antiparallel β-sheet is observed between β8 and C-linker (e.g., in the bacterial Htpg[5a]), which appears partially detached from the NTD. This suggests that the effects observed by NMR in solution are due to dynamic antiparallel strand formation of C-linker with β8.

The β8 strand in the Hsp90 NTD has a high content of hydrophobic residues, and the formation of a transient antiparallel β-hairpin with the C-linker might cause its detachment from the domain and the subsequent exposure of a binding site. This is consistent with previous observations of an increased affinity of the NTD for substrate peptides in the presence of the linker.[10] We found that the p53-DBD, a globular Hsp90 client, contacts the β8 strand of the NTD in the presence of the full linker, while substrate interactions are reduced in the absence of the linker. This supports the notion that linker interactions remove an autoinhibition of the β8 strand. Importantly, the contacts of p53 to β8 are very similar to those observed in the full-length Hsp90 protein, indicating the relevance of the NTD-linker for the binding properties of the chaperone.[22]

Mutations or deletions of N- and C-linker regions in Hsp90 have been previously found to induce overall conformational changes, especially affecting the relative orientation and rotational flexibility of the NTD,[9a,b] or the ability to reach closed conformations.[9b] In addition, deletion of the linker residues 211–259 substantially decreased the activation by the co-chaperone Aha1, although it did not interfere with the Hsp90 ATPase activity in its absence.[9a] This indicates an intimate connection between NTD-linker interactions and the overall conformational state of the Hsp90 dimer. Hence, certain steps of the conformational cycle of the Hsp90 chaperone that are triggered by nucleotides and/or co-chaperones are strongly sensitive to the linker contacts. More importantly, the fact that NTD-linker contacts increase the accessibility of a binding site in

the NTD suggests a mechanism for coupling Hsp90 conformation with binding to the NTD–MD interface. Interestingly, this interface participates in the interactions with the substrates p53 and Tau.[21b,22] The relevance of this site might be only required
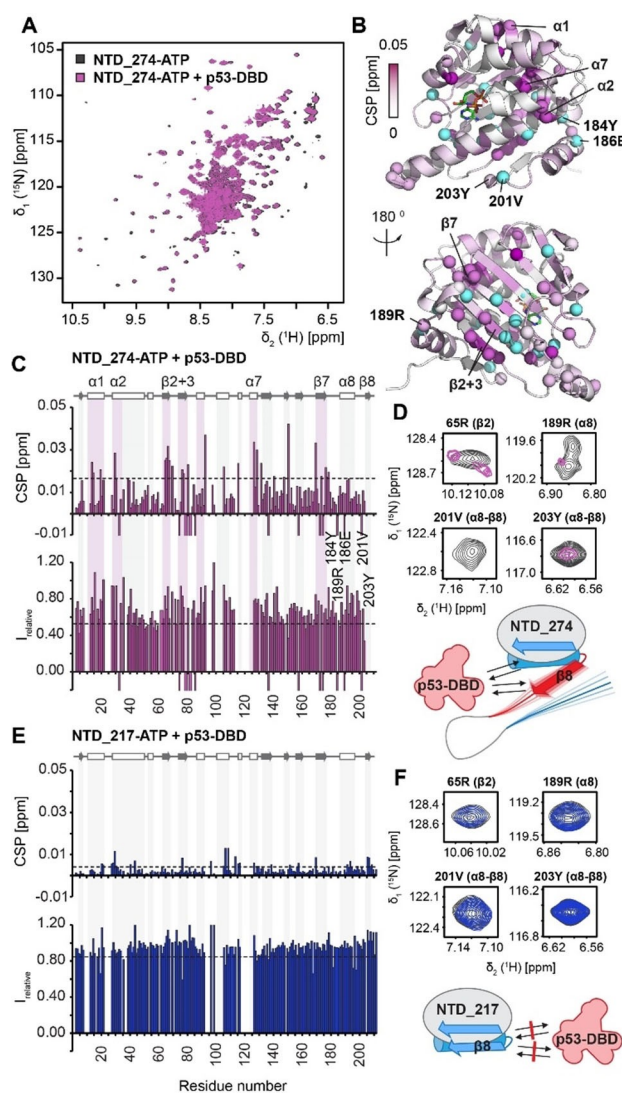

Figure 5. Detachment of the β8 strand in the Hsp90 NTD by C-linker interactions exposes hydrophobic residues that mediate interactions with clients. A) ^{1}H,^{15}N HSQC spectra of N274 bound to ATP (gray) and in complex with 1 equiv. of p53-DBD (purple). B), C) CSPs and intensity ratios vs. residue number of N274-ATP upon complex formation with p53-DBD (C). Regions experiencing bigger changes are highlighted in purple, and structural elements are indicated at the top. Residues of β8 and α8 showing variations are labeled. Median values +or−1σ are shown as dotted lines for CSP or relative intensities, respectively. The distribution of p53-DBD binding CSPs on the crystal structure of Hsp90 NTD bound to ATP (PDB ID: 1AM1,[20] nucleotide shown in green sticks) is shown in (B). Residues showing bigger CSPs or intensity changes are shown as spheres; residues experiencing line broadening are represented as cyan spheres. D) Zoomed views of residue signals located on β2, β8 and α8. A schematic representation of dynamic interaction of p53-DBD with β8 upon detachment by C-linker contacts is shown at the bottom. E) CSP and relative intensity plots of NTD_217 upon binding of p53-DBD. F) Zoomed views of the residues shown in (D) for the NTD_217 construct bound to ATP (gray) and in complex with 1 equiv. of p53 (blue). The absence of perturbations supports the role of the linker on releasing the autoinhibition of strand β8 (schematic representation at the bottom).

ChemBioChem

Full Papers
doi.org/10.1002/cbic.202000699

Chemistry
Europe
European Chemical
Societies Publishing

for certain client types, as demonstrated by the high dependency of chaperone activity on linker length and sequence for specific clients.[9a]

Conclusion

Taken together, our results highlight conformational features of the linker and interactions with the NTD that have a regulatory role. Linker regulation not only affects the structure and conformational dynamics of Hsp90, but is also required for interactions with co-chaperones and substrates. For this function, N- and C-linker regions are critical. In contrast, the negatively charged and unstructured mid-linker might have other functions, perhaps by enhancing solubility and stability of a wide variety of Hsp90 complexes. This is consistent with the prevalence of negatively charged linkers in Hsp90 of eukaryotes.

Our data highlight a regulatory role of the linker by modulating the accessibility of β8 of the NTD through a transient direct interaction. Such regulation is likely to be dependent on the overall conformation of Hsp90, nucleotides and co-chaperones. These results highlight that flexible linkers flanking and/or connecting globular domains can play important roles to modulate protein function.

Experimental Section

Cloning, protein expression and purification: NTD-linker extension constructs were designed by insertion of a stop codon to pET28a plasmid containing N-terminal His$_6$-SUMO-tagged NTD_MD construct of yeast Hsp90 (Hsp82). Linker-MD extension constructs were amplified by PCR from the same plasmid inserting NcoI and NotI restriction sites to the 5'- and 3'-ends, respectively. After digestion, the sequence was inserted to double digested pETM-11 vector. Isolated linker 210–283 was derived by introduction of a stop codon to 210_MD. Primers for stop codons and the E71Q mutant of N217 were designed with the help of the NEB base changer tool; all primers were purchased from Eurofins Genomics (Ebergsberg, Germany). Plasmids were transformed into *E. coli* BL21 DE3 cells, and cultures were grown in M9 minimal medium supplemented with ^{15}N-NH$_4$Cl for recording ^{1}H,^{15}N HSQC spectra, and in partially deuterated medium (85–75% D$_2$O) supplemented with ^{15}N NH$_4$Cl and ^{13}C-glucose for recording backbone resonance assignment experiments. In case of methyl labeled NTD_210 and NTD_MD constructs, cells were grown in fully deuterated M9 medium supplemented with ^{2}H glucose. Precursors for methyl labeling of Ile-Cδ1, Leu-Cδ, Met-Cε, Val-Cγ groups were added 1 h prior induction except for the NTD_MD construct, for which precursors for stereospecific labeling of pro-R groups were added according to the manufacturer's protocol (NMR-Bio, Grenoble, France). For the isolated linker, in which only double labeling was used. Proteins were expressed overnight at 25 °C after induction with 1 mM IPTG, and were purified as described previously.[26] In order to eliminate nucleic acid impurities on NTD constructs, an additional anion exchange chromatography step was included before gel filtration. Isolated linker purification takes advantage from the thermal stability, high solubility and low structural content of the protein. In brief, after resuspension of cell pellets in 50 mM Tris·HCl pH 8, 150 mM NaCl, 5 mM imidazole, complemented with protease inhibitor mixture (Roche), PMSF (Sigma-Aldrich), 100 μL of DNAse I

at 1 mg/mL and 1 mL of lysozyme at 100 mg/mL, cells were sonicated and the lysate was boiled in a water bath for 20 min. Afterwards, aggregated materials were removed by centrifugation. Nucleic acid impurities were precipitated by addition of streptomycin sulfate at a final concentration of 10 mg/mL followed by centrifugation. The protein was further purified from the clear supernatant by Ni-NTA affinity, reverse Ni-NTA after TEV cleavage, and by gel filtration. P53-DBD was expressed and purified as described in the literature.[27] The complex between NTD_274/NTD_217 and p53-DBD was prepared by adding ATP to the NTD, followed by mixing the two proteins in a 1:1 ratio, and buffer exchanging them to NMR buffer containing 2.5 mM DTT by three cycles of concentration/dilution using a centrifuge concentrator.

NMR spectroscopy: All NMR experiments were performed in Bruker 500 and 600 MHz spectrometers equipped with cryogenically cooled probes (Bruker Biospin), with the exception backbone assignment experiments of NTD_274 and 210_MD and the 3D CCH-NOESY of NTD_210 and NTD_MD which were recorded at 950 MHz. All NMR samples consisted of 150–250 μM of protein in 20 mM sodium phosphate pH 6.5, 100 mM NaCl, 5 mM MgCl$_2$ and 0.02% of sodium azide containing 10% of D$_2$O. For the ATP-bound experiments, 5 mM of ATP from a 100x pH-corrected stock was added. Methyl labeled samples were recorded in D$_2$O buffer containing 20 mM ^{2}H$_{11}$-Tris·HCl pH 7 (uncorrected pH-meter reading), 100 mM NaCl, 5 mM MgCl$_2$. ^{1}H,^{15}N HSQC experiments with watergate flip-back suppression of water signal were recorded at 25 °C; a combination of triple-resonance HNCACB, CBCACONH, HNCO and HNCACO experiments were recorded for the linker assignment with a high number of increments on the indirect dimensions and using non-uniform sampling. For N- and M-extension constructs, HNCACB and HNCACO experiments were recorded for confirming assignment transfers from the isolated linker. Spectra were processed by NMRPipe[28] and analyzed by CCPnmr software.[29] The following formula was used for extracting CSPs, which takes into consideration the ^{1}H chemical-shift range of NMR signals:

$$\Delta\delta_{N,H}\,(\text{ppm}) = \sqrt{\Delta\delta_H^2 + (\alpha \cdot \Delta\delta_N)^2}$$

Where α is a scaling factor calculated from the ratio between the ^{1}H and ^{15}N chemical shift ranges, with an approximate value of 0.16 for a folded protein, and of 0.05 for a disordered protein. {^{1}H}^{15}N steady-state heteronuclear NOE experiments were performed by using modified sequences described by Farrow et al.[30] by collecting two datasets, one without no ^{1}H saturation and a second with an initial ^{1}H saturation, in an interleaved fashion. Heteronuclear NOE values were obtained from the intensity ratio of backbone resonances between the saturated and unsaturated spectra, and errors were estimated from spectral baseplane noise RMSD as described by Farrow et al.[30] Residual secondary structure was extracted from deviations in the experimental ^{13}C chemical shifts of Cα, Cβ and C' using the following formula: $\Delta\delta$Cα, Cβ, C'$_i$ = $(\delta C\alpha_i - \delta C\alpha_{r.c.}) - (\delta C\beta_i - \delta C\beta_{r.c.}) + (\delta C'_i - \delta C'_{r.c.})$, where $\delta C\alpha_{r.c.}$, $\delta C\beta_{r.c.}$ and $\delta C'_{r.c.}$ are the random-coil ^{13}C values determined by Wishart et al.[31] ^{15}N-edited NOESY experiments were performed with a mixing time of 120 ms.

Isothermal titration calorimetry: ITC experiments were performed in a MicroCal PEAQ-ITC instrument (Malvern Panalytical, Malvern, UK). Protein was contained in the cell, and the nucleotide was titrated from the syringe at 25 °C. A protein concentration of 75 M was used for NTD_217 and NTD_274 constructs, with a ligand concentration of 1.5 mM. Both samples were in HEPES-KOH pH 7.5, 150 mM KCl, 5 mM MgCl$_2$; pH was corrected for the nucleotide solution. A total number of 26 injection points of 1.5 μL were performed separated by 150 s. Data were analyzed with the

ChemBioChem

Full Papers
doi.org/10.1002/cbic.202000699

**Chemistry
Europe**
European Chemical
Societies Publishing

commercial MicroCal PEAQ-ITC V1.21 software, using least-squares deconvolution fitting to one set of sites and treating number of sites, dissociation constant K_D, and enthalpy variation of binding $\Delta H°$ as variables. In these conditions, high quality data were obtained for ADP, but acceptable results could not be achieved for ATP.

Conflict of Interest

The authors declare no conflict of interest.

[1] F. H. Schopf, M. M. Biebl, J. Buchner, *Nat. Rev. Mol. Cell Biol.* **2017**, *18*, 345–360.

[2] a) M. Hessling, K. Richter, J. Buchner, *Nat. Struct. Mol. Biol.* **2009**, *16*, 287–293; b) M. M. U. Ali, S. Mark Roe, C. K. Vaughan, P. Meyer, B. Panaretou, P. W. Piper, C. Prodromou, L. H. Pearl, *Nature* **2006**, *440*, 1013–1017; c) C. Prodromou, B. Panaretou, S. Chohan, G. Siligardi, R. O'Brien, J. E. Ladbury, S. M. Roe, P. W. Piper, L. H. Pearl, *EMBO J.* **2000**, *19*, 4383–4392.

[3] D. R. Southworth, D. A. Agard, *Mol. Cell* **2008**, *32*, 631–640.

[4] B. K. Zierer, M. Rübbelke, F. Tippel, T. Madl, F. H. Schopf, D. A. Rutz, K. Richter, M. Sattler, J. Buchner, *Nat. Struct. Mol. Biol.* **2016**, *23*, 1020–1028.

[5] a) A. K. Shiau, S. F. Harris, D. R. Southworth, D. A. Agard, *Cell* **2006**, *127*, 329–340; b) S. Tsutsumi, M. Mollapour, C. Prodromou, C. T. Lee, B. Panaretou, S. Yoshida, M. P. Mayer, L. M. Neckers, *Proc. Natl. Acad. Sci. USA* **2012**, *109*, 2937–2942.

[6] a) M. Kurokawa, C. Zhao, T. Reya, S. Kornbluth, *Mol. Cell. Biol.* **2008**, *28*, 5494; b) H. Ogiso, N. Kagi, E. Matsumoto, M. Nishimoto, R. Arai, M. Shirouzu, J. Mimura, Y. Fujii-Kuriyama, S. Yokoyama, *Biochemistry* **2004**, *43*, 15510–15519.

[7] a) M. Jahn, A. Rehn, B. Pelz, B. Hellenkamp, K. Richter, M. Rief, J. Buchner, T. Hugel, *Proc. Natl. Acad. Sci. USA* **2014**, *111*, 17881–17886; b) O. Hainzl, M. C. Lapina, J. Buchner, K. Richter, *J. Biol. Chem.* **2009**, *284*, 22559–22567.

[8] K. A. Verba, R. Y. R. Wang, A. Arakawa, Y. Liu, M. Shirouzu, S. Yokoyama, D. A. Agard, *Science* **2016**, *352*, 1542–1547.

[9] a) S. Daturpalli, R. A. Knieß, C. T. Lee, M. P. Mayer, *J. Mol. Biol.* **2017**, *429*, 1406–1423; b) M. Jahn, A. Rehn, B. Pelz, B. Hellenkamp, K. Richter, M. Rief, J. Buchner, T. Hugel, *Proc. Natl. Acad. Sci. USA* **2014**, *111*, 17881–17886; c) B. Hellenkamp, P. Wortmann, F. Kandzia, M. Zacharias, T. Hugel, *Nat. Methods* **2017**, *14*, 176–182.

[10] T. Scheibel, H. I. Siegmund, R. Jaenicke, P. Ganz, H. Lilie, J. Buchner, *Proc. Natl. Acad. Sci. USA* **1999**, *96*, 1297–1302.

[11] S. Tsutsumi, M. Mollapour, C. Graf, C.-T. Lee, B. T. Scroggins, W. Xu, L. Haslerova, M. Hessling, A. A. Konstantinova, J. B. Trepel, B. Panaretou, J.

[12] a) T. N. Cordeiro, N. Sibille, P. Germain, P. Barthe, A. Boulahtouf, F. Allemand, R. Bailly, V. Vivat, C. Ebel, A. Barducci, W. Bourguet, A. le Maire, P. Bernadó, *Structure* **2019**, *27*, 1270–1285.e1276; b) H.-S. Kang, C. Sánchez-Rico, S. Ebersberger, F. X. R. Sutandy, A. Busch, T. Welte, R. Stehle, C. Hipp, L. Schulz, A. Buchbender, K. Zarnack, J. König, M. Sattler, *Proc. Natl. Acad. Sci. USA* **2020**, *117*, 7140; c) J. D. Walsh, K. Meier, R. Ishima, A. M. Gronenborn, *Biophys. J.* **2010**, *99*, 2636–2646; d) J.-r. Huang, L. R. Warner, C. Sanchez, F. Gabel, T. Madl, C. D. Mackereth, M. Sattler, M. Blackledge, *J. Am. Chem. Soc.* **2014**, *136*, 7068–7076; e) N. E. Davey, *Curr. Opin. Struct. Biol.* **2019**, *56*, 155–163.

[13] P. Mier, L. Paladin, S. Tamana, S. Petrosian, B. Hajdu-Soltész, A. Urbanek, A. Gruca, D. Plewczynski, M. Grynberg, P. Bernadó, Z. Gáspári, C. A. Ouzounis, V. J. Promponas, A. V. Kajava, J. M. Hancock, S. C. E. Tosatto, Z. Dosztanyi, M. A. Andrade-Navarro, *Briefings Bioinf.* **2020**, *21*, 458–472.

[14] A. Waterhouse, M. Bertoni, S. Bienert, G. Studer, G. Tauriello, R. Gumienny, F. T. Heer, T. A. P. de Beer, C. Rempfer, L. Bordoli, R. Lepore, T. Schwede, *Nucleic Acids Res.* **2018**, *46*, W296-W303.

[15] J. Kyte, R. F. Doolittle, *J. Mol. Biol.* **1982**, *157*, 105–132.

[16] F. Glaser, T. Pupko, I. Paz, R. E. Bell, D. Bechor-Shental, E. Martz, N. Ben-Tal, *Bioinformatics* **2003**, *19*, 163–164.

[17] D. T. Jones, *J. Mol. Biol.* **1999**, *292*, 195–202.

[18] A. Drozdetskiy, C. Cole, J. Procter, G. J. Barton, *Nucleic Acids Res.* **2015**, *43*, W389-W394.

[19] a) R. M. Salek, M. A. Williams, C. Prodromou, L. H. Pearl, J. E. Ladbury, *J. Biomol. NMR* **2002**, *23*, 327–328; b) A. Dehner, J. Furrer, K. Richter, I. Schuster, J. Buchner, H. Kessler, *ChemBioChem* **2003**, *4*, 870–877; c) F. Hagn, S. Lagleder, M. Retzlaff, J. Rohrberg, O. Demmer, K. Richter, J. Buchner, H. Kessler, *Nat. Struct. Mol. Biol.* **2011**, *18*, 1086–1093.

[20] C. Prodromou, S. M. Roe, R. O'Brien, J. E. Ladbury, P. W. Piper, L. H. Pearl, *Cell* **1997**, *90*, 65–75.

[21] a) G. E. Karagoz, A. M. Duarte, E. Akoury, H. Ippel, J. Biernat, T. Moran Luengo, M. Radli, T. Didenko, B. A. Nordhues, D. B. Veprintsev, C. A. Dickey, E. Mandelkow, M. Zweckstetter, R. Boelens, T. Madl, S. G. Rudiger, *Cell* **2014**, *156*, 963–974; b) J. Oroz, B. J. Chang, P. Wysoczanski, C.-T. Lee, Á. Pérez-Lara, P. Chakraborty, R. V. Hofele, J. D. Baker, L. J. Blair, J. Biernat, H. Urlaub, E. Mandelkow, C. A. Dickey, M. Zweckstetter, *Nat. Commun.* **2018**, *9*, 4532.

[22] S. J. Park, M. Kostic, H. J. Dyson, *J. Mol. Biol.* **2011**, *411*, 158–173.

[23] O. R. Lorenz, L. Freiburger, D. A. Rutz, M. Krause, B. K. Zierer, S. Alvira, J. Cuéllar, T. Valpuesta, T. Madl, M. Sattler, J. Buchner, *Mol. Cell* **2014**, *53*, 941–953.

[24] a) M. A. Martinez-Yamout, R. P. Venkitakrishnan, N. E. Preece, G. Kroon, P. E. Wright, H. J. Dyson, *J. Biol. Chem.* **2006**, *281*, 14457–14464; b) G. E. Karagoz, A. M. Duarte, H. Ippel, C. Uetrecht, T. Sinnige, M. van Rosmalen, J. Hausmann, J. A. Heck, R. Boelens, S. G. Rudiger, *Proc. Natl. Acad. Sci. USA* **2011**, *108*, 580–585.

[25] M. Retzlaff, F. Hagn, L. Mitschke, M. Hessling, F. Gugel, H. Kessler, K. Richter, J. Buchner, *Mol. Cell* **2010**, *37*, 344–354.

[26] S. L. Mader, A. Lopez, J. Lawatscheck, Q. Luo, D. A. Rutz, A. P. Gamiz-Hernandez, M. Sattler, J. Buchner, V. R. I. Kaila, *Nat. Commun.* **2020**, *11*, 1410.

[27] V. Dahiya, G. Agam, J. Lawatscheck, D. A. Rutz, D. C. Lamb, J. Buchner, *Mol. Cell* **2019**, *74*, 816–830 e817.

[28] F. Delaglio, S. Grzesiek, G. W. Vuister, G. Zhu, J. Pfeifer, A. Bax, *J. Biomol. NMR* **1995**, *6*, 277–293.

[29] W. F. Vranken, W. Boucher, T. J. Stevens, R. H. Fogh, A. Pajon, M. Llinas, E. L. Ulrich, J. L. Markley, J. Ionides, E. D. Laue, *Proteins Struct. Funct. Bioinf.* **2005**, *59*, 687–696.

[30] N. A. Farrow, R. Muhandiram, A. U. Singer, S. M. Pascal, C. M. Kay, G. Gish, S. E. Shoelson, T. Pawson, J. D. Forman-Kay, L. E. Kay, *Biochemistry* **1994**, *33*, 5984–6003.

[31] D. S. Wishart, C. G. Bigam, A. Holm, R. S. Hodges, B. D. Sykes, *J. Biomol. NMR* **1995**, *5*, 67–81.